REPORT DOCUMENTATION PAGE

Form Approved
OMB No. 0704-0188

PLEASE DO NOT RETURN YOUR FORM TO THE ABOVE ADDRESS.

1. REPORT DATE *(DD-MM-YYYY)*	2. REPORT TYPE	3. DATES COVERED
14-02-2006	FINAL	Jun 2001 - Feb 2006

4. TITLE AND SUBTITLE

Long-Term Durability and Damage Tolerance of Innovative Marine Composites

5a. CONTRACT NUMBER

5b. GRANT NUMBER
N00014-01-1-0949

5c. PROGRAM ELEMENT NUMBER

6. AUTHOR(S)

Miyano, Yasushi
Kimpara, Isao
and others

5d. PROJECT NUMBER

5e. TASK NUMBER

5f. WORK UNIT NUMBER

7. PERFORMING ORGANIZATION NAME(S) AND ADDRESS(ES)

Kanazawa Institute of Technology
Materials System Research Laboratory
3-1 Yatsukaho, Hakusan, Ishikawa 924-0838 Japan

8. PERFORMING ORGANIZATION REPORT NUMBER
KIT-MSRL-06-01

9. SPONSORING/MONITORING AGENCY NAME(S) AND ADDRESS(ES)

Office of Naval Research
Balliston Centre Tower One
800 North Quincy St. Arlington VA 22127-5660

10. SPONSOR/MONITOR'S ACRONYM(S)
ONR

11. SPONSOR/MONITOR'S REPORT NUMBER(S)

12. DISTRIBUTION/AILABILITY STATEMENT

Approved for Public Release, Distribution is Unlimited.

13. SUPPLEMENTARY NOTES

14. ABSTRACT

The prediction of long-term fatigue life of innovative CFRP laminates for marine use under temperature and water environments were performed by our developed accelerated testing methodology based on the time-temperature superposition principle. Furthermore, Mode I and Mode II interlaminar fracture toughness and the crack growth property under fatigue, thermal and water environments of innovative CFRP laminates were investigated.

15. SUBJECT TERMS

CFRP, Fatigue, Time-temperature superposition principle, Interlaminar fracture toughness, Crack growth, Thermal and water environments

16. SECURITY CLASSIFICATION OF:			17. LIMITATION OF ABSTRACT	18. NUMBER OF PAGES	19a. NAME OF RESPONSIBLE PERSON
a. REPORT	b. ABSTRACT	c. THIS PAGE			Nobumasa Iwashita
U	U	U	UU	22	19b. TELEPHONE NUMBER *(Include area code)* +81 76 294 6719

Long-Term Durability and Damage Tolerance of Innovative Marine Composites

Final Report

Part I : Accelerated Testing for Long-Term Durability of Innovative CFRP Laminates for Marine Use

Yasushi Miyano and Masayuki Nakada

Materials System Research Laboratory, Kanazawa Institute of Technology, 3-1 Yatsukaho, Hakusan, Ishikawa 924-0838, Japan

OBJECTIVE

The prediction of long-term fatigue life of innovative CFRP laminates for marine use under temperature and water environments were performed by our developed accelerated testing methodology based on the time-temperature superposition principle (TTSP).

APPROACH

Three kinds of CFRP laminates employed were conventional plain fabric T300 carbon fibers/vinylester, flat yarn plain fabric T700 carbon fibers/vinylester and multi-axial knitted T700 carbon fibers/vinylester for marine use. These CFRP laminates were prepared under three water absorption conditions of Dry, Wet and Wet+Dry after molding. The three-point bending constant strain rate (CSR) tests for three kinds of CFRP laminates at three conditions of water absorption were carried out at various temperatures and strain rates. Furthermore, the three-point bending fatigue tests for these specimens were carried out at various temperatures and frequencies.

RECENT ACHIEVEMENTS

The flexural CSR and fatigue strengths of these CFRP laminates strongly depend on water absorption as well as time and temperature. The mater curves of fatigue strength as well as CSR strength for these CFRP laminates at these conditions are constructed by using the test data based on TTSP. It is possible to predict the long term fatigue life for these CFRP laminates under an arbitrary temperature and water absorption conditions by using the master curves.

1. Introduction

Recently carbon fiber reinforced plastics (CFRP) has been used for the primary structures of airplanes, ships, spacecrafts and others, in which the high reliability should be kept during the long-term operation. Therefore, it is strongly expected that the accelerated testing methodology for the long-term life prediction of composite structures exposed under the actual environments of temperature, water, and others is established.

The mechanical behavior of polymer resins exhibits time and temperature dependence, called viscoelastic behavior, not only above the glass transition temperature T_g but also below T_g [1-8]. Furthermore, the viscoelastic behavior of polymer resins also depends on the water absorption [9-12]. Thus, it can be presumed that the mechanical behavior of polymer composites significantly depends on the water absorption as well as time and temperature.

This paper is concerned with the prediction of long-term fatigue life of innovative CFRP laminates for marine use under temperature and water environments. Three kinds of CFRP laminates employed were conventional plain fabric T300 carbon fibers/vinylester, flat yarn plain fabric T700 carbon fibers/vinylester and multi-axial knitted T700 carbon fibers/vinylester for marine use. These CFRP laminates were prepared under three water absorption conditions of Dry, Wet and Wet+Dry after molding. The three-point bending constant strain rate (CSR) tests for three kinds of CFRP laminates at three conditions of water absorption were carried out at various temperatures and strain rates. Furthermore, the three-point bending fatigue tests for these specimens were carried out at various temperatures and frequencies. The time, temperature, and water absorption dependencies of flexural fatigue strength as well as flexural CSR strength for these CFRP laminates are discussed based on TTSP.

2. Experimental Procedures

Preparation of specimens

Three kinds of CFRP laminates employed were conventional plain fabric T300 carbon fibers/vinylester (T300/VE), flat yarn plain fabric T700 carbon fibers/vinylester (T700/VE:F) and multi-axial knitted T700 carbon fibers/vinylester (T700/VE:K) for marine use. These CFRP laminates were formed by resin transfer molding (RTM). All of CFRP laminates was cured at room temperature over 24 hours. The fiber volume fraction was approximately 51%. The thickness of the laminates was 2mm.

These CFRP laminates were prepared under three water absorption conditions of Dry, Wet and Wet+Dry after molding. Dry specimens by holding the cured specimens at 150°C for 2 hours in air, Wet specimens by soaking Dry specimens in hot water of 95°C for 120 hours and Wet+Dry specimens by dehydrating the Wet specimens at 150°C for 2 hours in air were respectively prepared as shown in Table 1. The water contents of Dry and Wet+Dry specimens were 0% and that of Wet specimen was 0.6%.

Table 1 Preparing conditions for Dry, Wet, and Wet+Dry specimens

	Water content	In air	In water	In air
Dry	0%	150°C x 2h	-	-
Wet	0.6%	150°C x 2h +	95°C x 120h	-
Wet+Dry	0%	150°C x 2h +	95°C x 120h +	150°C x 2h

Experimental procedures

To evaluate the viscoelastic behavior of matrix vinylester (VE) resin, the three-point bending creep tests for the neat vinylester resin prepared at Dry, Wet and Wet+Dry conditions were carried out under various temperatures using an creep testing machine with temperature chamber. The creep compliance D_c was calculated from the deflection δ at the center of specimen using the following equation:

$$D_c = \frac{4bh^3\delta}{P_0 L^3} \tag{1}$$

where P_0 is the applied constant load (58.8N), L is the span (50mm), and b and h are the width (25mm) and the thickness (3.0mm) of specimen, respectively.

The three-point bending CSR tests for three kinds of CFRP laminates at Dry, Wet and Wet+Dry conditions were carried out at various temperatures and strain rates. The span is L=60mm, and the width and thickness are b=15mm and h=2.0mm, respectively. The CSR tests were conducted at three loading-rates V=0.02, 2, 200 mm/min and various constant temperatures T using an universal testing machine with temperature chamber. The flexural CSR strength σ_s is calculated from the maximum load P_s by

$$\sigma_s = \frac{3P_s L}{2bh^2}. \tag{2}$$

Furthermore, the three-point bending fatigue tests for these specimens were carried out at various constant temperatures T and two loading frequencies f=2Hz and 0.02Hz using an electro-hydraulic servo testing machine with temperature chamber. The stress ratio R (= minimum stress/maximum stress) was 0.05. The length, width, thickness of specimen, and span are the same to those for the flexural CSR tests. The flexural fatigue strength σ_f is defined by maximum applied load P_{max} for the number of cycles to failure N_f.

$$\sigma_f = \frac{3P_{max} L}{2bh^2}. \tag{3}$$

In order to prevent the dryness of specimens at Wet condition during creep, CSR, and fatigue tests, the specimens were wrapped by a vinyl bag with including distilled water in the bag.

3. Results and Discussion

Creep compliance

The left side of Fig.1 shows the creep compliance D_c versus testing time t at various temperatures T for Dry, Wet and Wet+Dry specimens of VE resin. The master curves of D_c versus the reduced time t' were constructed by shifting D_c at various constant temperatures along the log scale of t and the log scale of D_c. Since the smooth master curve of D_c for each specimen can be obtained as shown in the right side of each graph, the time-temperature superposition principle (TTSP) is applicable for each D_c. From Fig.1 (b) and (c), it is cleared that D_c increases with water absorption and returns perfectly to that of Dry specimen by re-drying after water absorption.

The horizontal time-temperature shift factor $a_{T_0}(T)$ and the vertical temperature shift factor $b_{T_0}(T)$ at a reference temperature T_0 plotted in Fig.2 are respectively defined by

$$\log a_{T_0}(T) = \log t - \log t' \tag{4}$$

$$\log b_{T_0}(T) = \log D_c(t,T) - \log D_c(t',T_0) \tag{5}$$

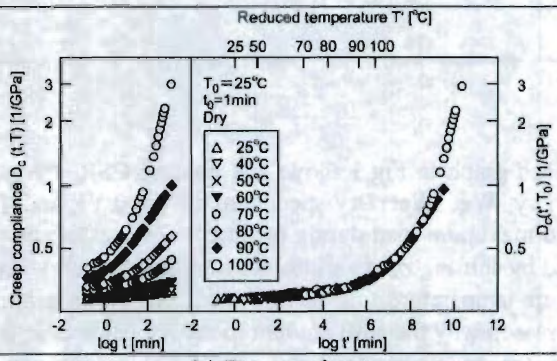

(a) Dry specimen

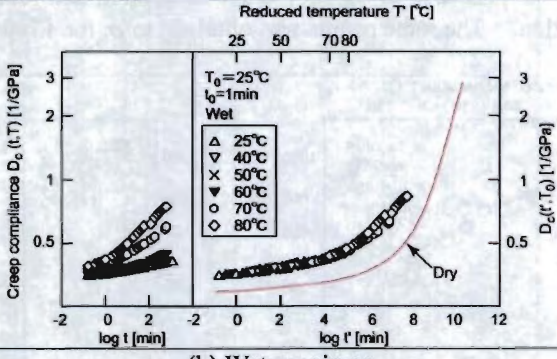

(b) Wet specimen

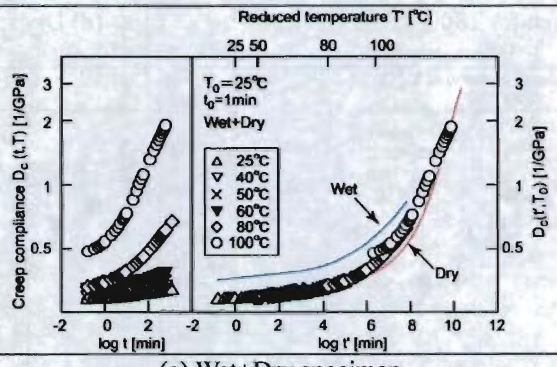

(c) Wet+Dry specimen

Fig.1 Master curves of creep compliance for VE resin

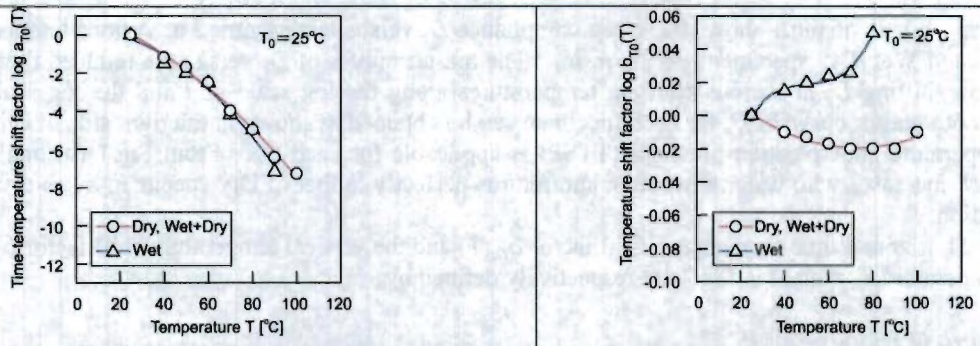

(a) Time-temperature shift factors $a_{T0}(T)$ **(b) Temperature shift factors $b_{T0}(T)$**

Fig.2 Time-temperature shift factors and temperature shift factors of creep compliance for VE resin

Flexural CSR strength

The left side of each graph in Fig.3 shows the flexural CSR strength σ_s versus time to failure t_s at various temperatures T for Dry, Wet, Wet+Dry specimens of T300/VE and T700/VE:F, where t_s is the time period from initial loading to maximum load during testing. The master curves of σ_s versus the reduced time to failure t_s' were constructed by shifting σ_s at various constant temperatures along the log scale of t_s and the log scale of σ_s using the same time-temperature shift factors and a half of the temperature shift factors for D_c of VE resin shown in Fig.2. The reason why the shift amount to the log scale of σ_s is a half of that to the log scale of D_c is mentioned after. Since the smooth master curve of σ_s for each specimen can be obtained as shown in the right side of each graph, the TTSP for D_c of VE resin is also applicable for each σ_s. It is cleared from Fig.3 that σ_s for T300/VE and T700/VE:F decreases with water absorption and returns to that of Dry specimen by re-drying after water absorption. The same results was obtained to σ_s for T700/VE:K.

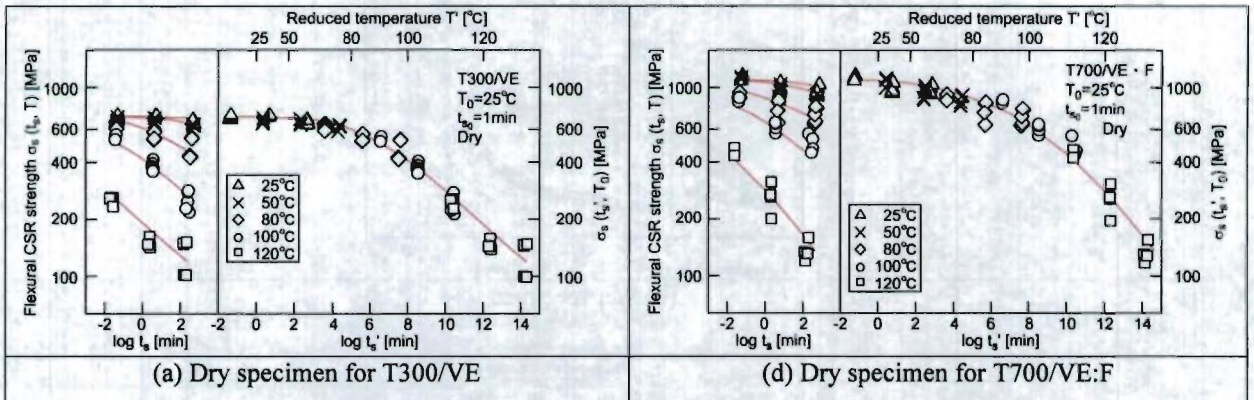

(a) Dry specimen for T300/VE (d) Dry specimen for T700/VE:F

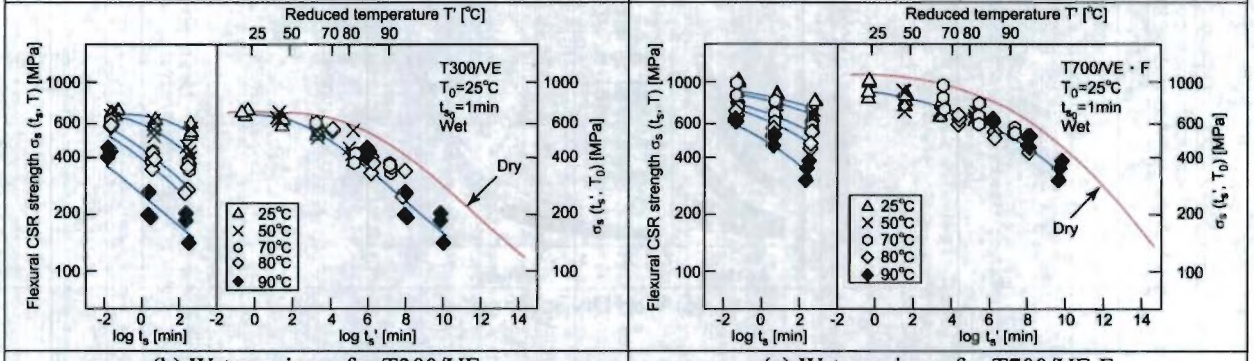

(b) Wet specimen for T300/VE (e) Wet specimen for T700/VE:F

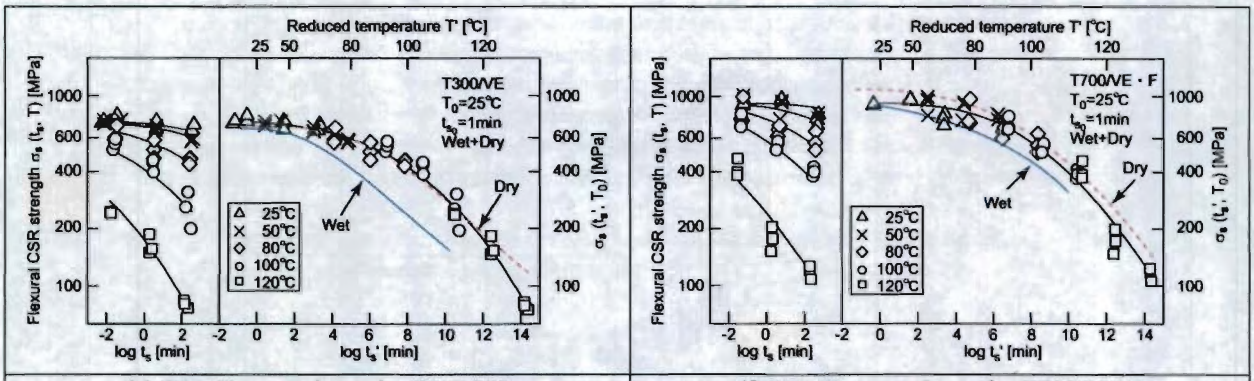

(c) Wet+Dry specimen for T300/VE

(f) Wet+Dry specimen for T700/VE:F

Fig.3 Master curves of flexural CSR strength for T300/VE and T700/VE:F

Fig. 4 shows the master curves of σ_s for Dry and Wet specimens of T300/VE, T700/VE:F, and T700/VE:K. It is cleared from this graph that the flexural CSR strength of these CFRP laminates strongly decreases with increasing the water absorption as well as time and temperature.

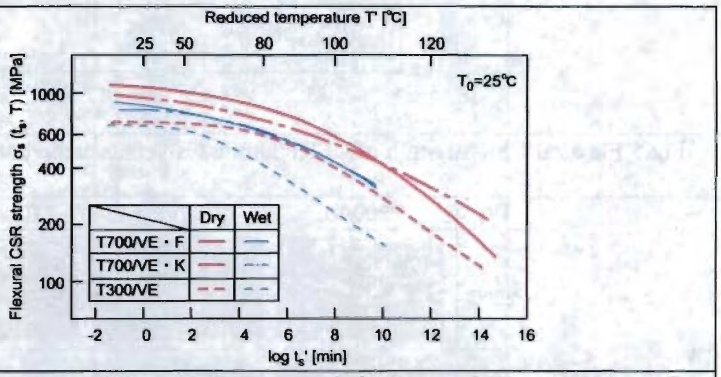

Fig.4 Master curves of flexural CSR strength for Dry and Wet specimens of T300/VE, T700/VE:F, and T700/VE:K

Fig. 5 shows the flexural CSR strength of T300/VE, T700/VE:F and T700/VE:K versus the creep compliance of matrix resin for Dry and Wet conditions. The degradation of flexural CSR strength for these CFRP laminates is uniquely determined by the creep compliance of matrix resin. Therefore, the degradation rate of flexural CSR strength of these CFRP laminates is determined only by increasing of time, temperature and water absorption and is independent upon fiber constitutions which are the type, volume fraction and weaves. The slope is approximately 0.5 shown in each graph of this figure. This indicates that the trigger of failure is the microbuckling of carbon fibers in the compression side of specimen shown by the following equation based on Dow's theory [13]:

$$\log \sigma_s = \log K' - \frac{1}{2} \log D_c \tag{6}$$

where σ_s is the CSR strength of CFRP laminates and D_c is the creep compliance of matrix resin. Actually, the fracture appearance shown in Fig.6 indicates that the fracture mode for these CFRP laminates is the compressive fracture of warp carbon fibers in the compression side of specimen for all condition tested. Therefore, this is the reason why the vertical shift amount for σ_s is a half of that for D_c as mentioned above.

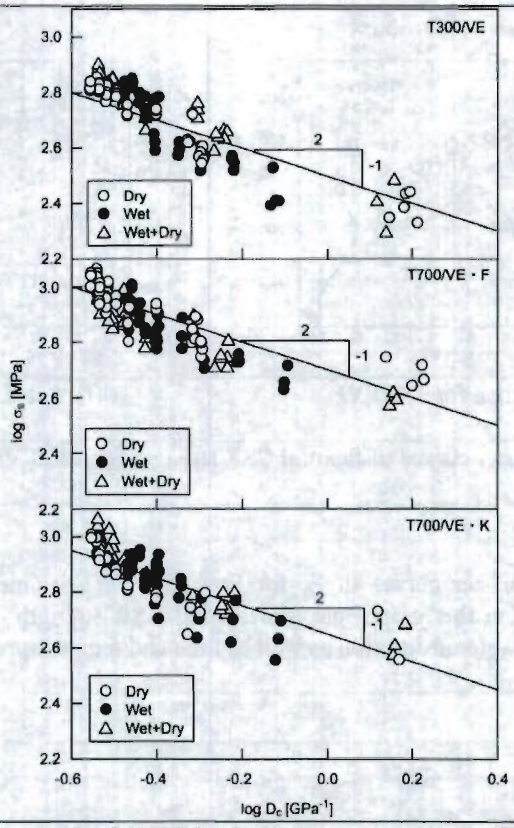

Fig.5 Flexural CSR strength of CFRP laminates versus creep compliance of matrix resin

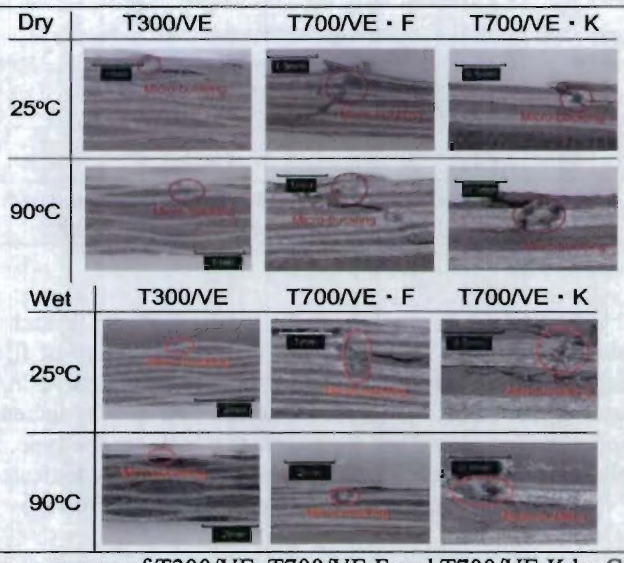

Fig. 6 Fracture appearance of T300/VE, T700/VE:F and T700/VE:K by CSR bending tests

Flexural fatigue strength

To describe the master curve of flexural fatigue strength σ_f, we need the reduced frequency f' in addition to the reduced time to failure t_f', each defined by

$$f' = f \cdot a_{T_0}(T) \ , \qquad t_f' = \frac{t_f}{a_{T_0}(T)} = \frac{N_f}{f'} \tag{7}$$

where N_f is the number of cycles to failure.

The σ_f versus N_f at frequency f=2Hz for Dry and Wet specimens of T300/VE and T700/VE:F are shown in Fig.7 where σ_f at N_f=1/2 is represented by σ_s at $t_s=(2f)^{-1}$. On the upper figure of each graph in Fig.8, σ_f versus

t_f' curves for several f' at T_0 are depicted by solid lines, which are obtained by converting N_f on Fig.8 into t_f' using Eq.(7), the time-temperature shift factors $a_{T_0}(T)$ and temperature shift factors $b_{T_0}(T)$ of CSR strength for each specimen. The master curves of σ_f for fixed N_f indicated by solid lines in the lower figure are constructed by connecting the points of the same N_f on the curves of each f' indicated by dotted lines in this figure.

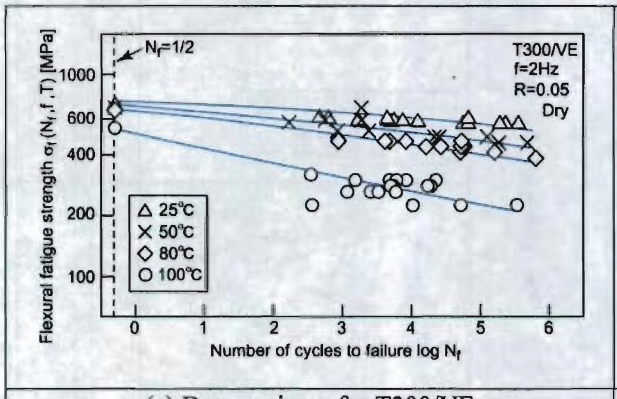

(a) Dry specimen for T300/VE

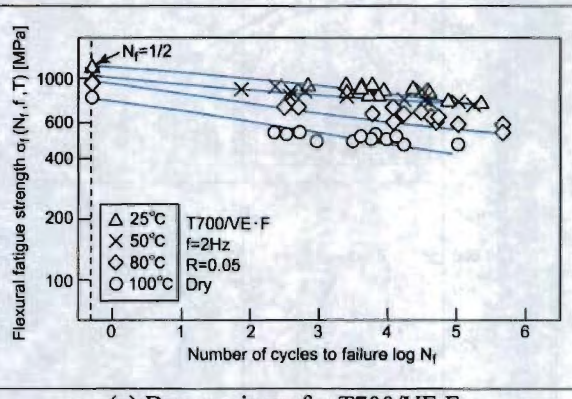

(c) Dry specimen for T700/VE:F

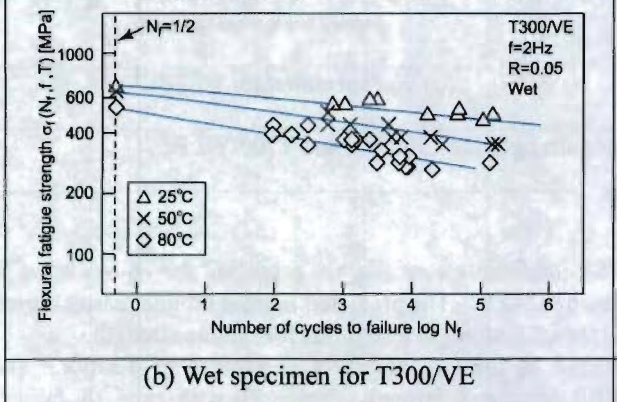

(b) Wet specimen for T300/VE

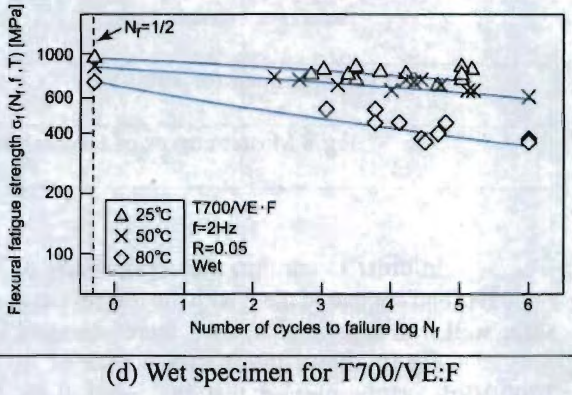

(d) Wet specimen for T700/VE:F

Fig.7 Flexural fatigue strength versus number of cycles to failure for frequency f= 2Hz for T300/VE and T700/VE:F

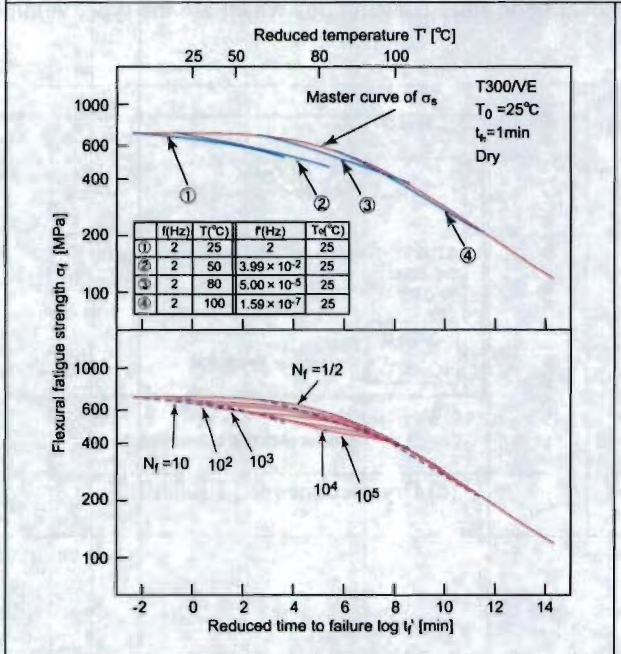

(a) Dry specimen for T300/VE

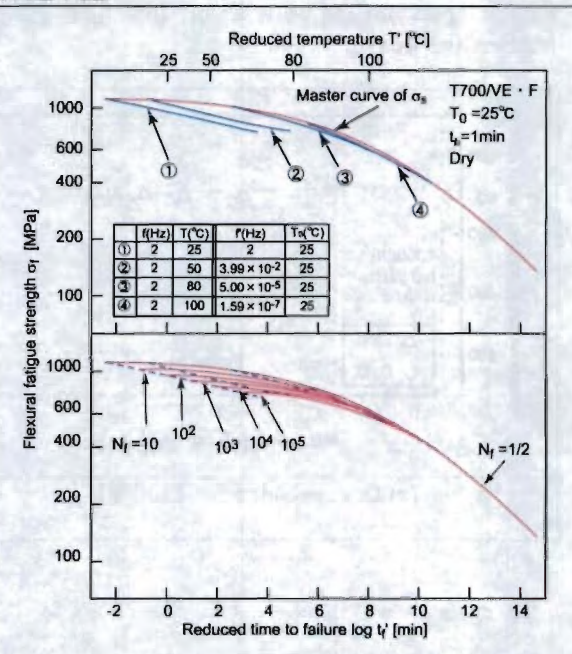

(c) Dry specimen for T700/VE:F

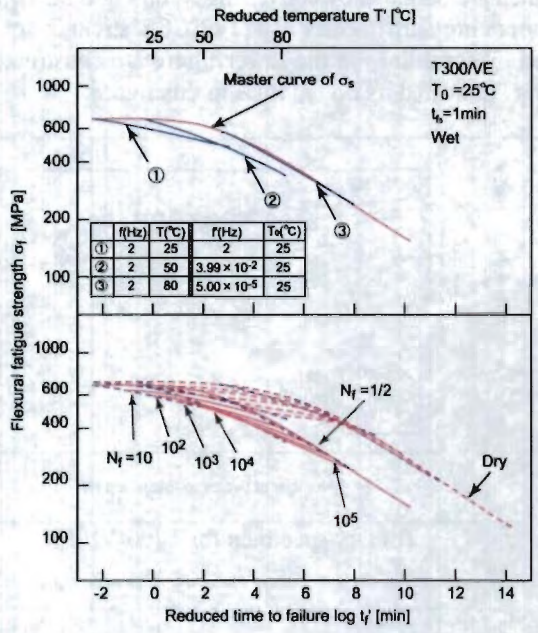

(b) Wet specimen for T300/VE

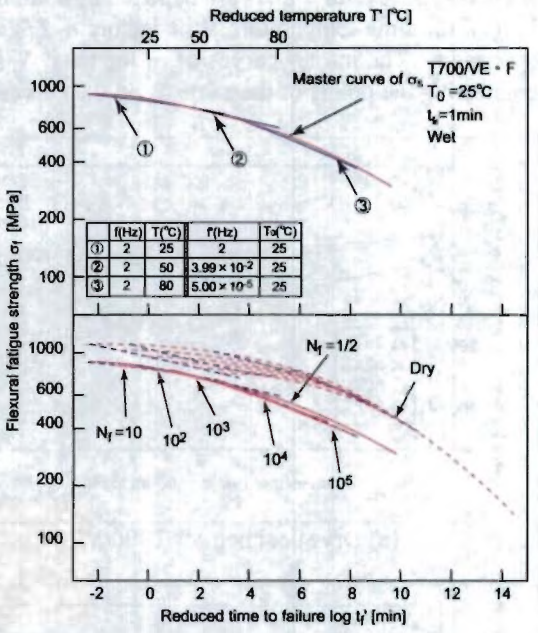

(d) Wet specimen for T700/VE:F

Fig.8 Master curves of flexural fatigue strength for T300/VE and T700/VE:F

In order to confirm the applicability of TTSP for fatigue strength, we predicted the σ_f-N_f curves at f=0.02Hz and compared them with the test results as shown in Fig.9. The predicted σ_f from fatigue master curves agree well with experimental ones, therefore, the TTSP for CSR strength also holds for fatigue strength.

Fig.10 shows the master curves of normalized σ_f for Dry and Wet specimens of T300/VE and T700/VE:F. It is cleared that the σ_f of these CFRP laminates strongly decreases with time to failure, temperature and water absorption, however decreases scarcely with N_f. And the degradation rate of fatigue strength of these CFRP laminates is the same to each other, therefore, this is determined only by increasing of time, temperature and water absorption and is independent upon fiber constitutions which are the type, volume fraction and weaves.

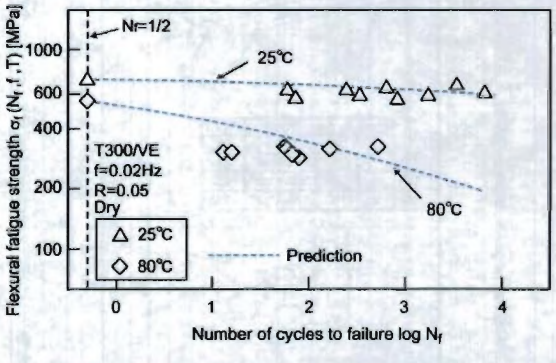

(a) Dry specimen for T300/VE

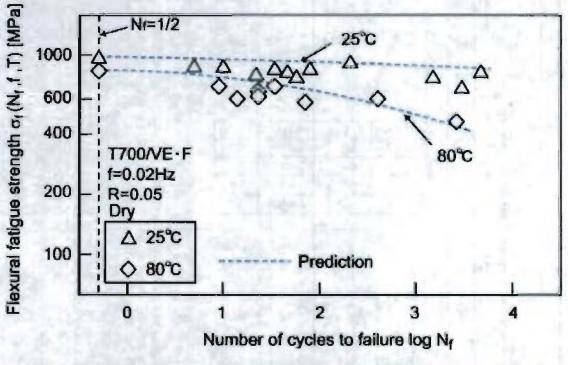

(c) Dry specimen for T700/VE:F

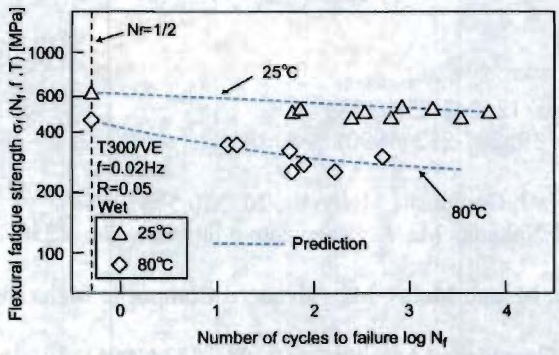

(b) Wet specimen for T300/VE

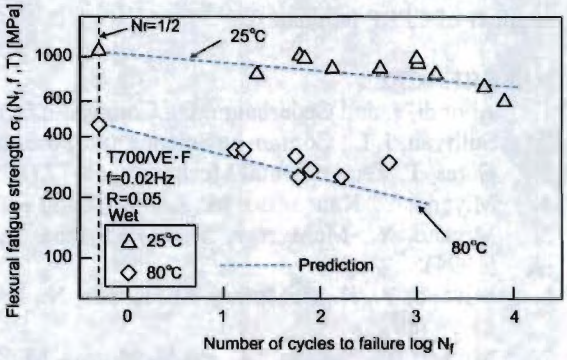

(d) Wet specimen for T700/VE:F

Fig.9 Flexural fatigue strength versus number of cycles to failure for frequency f= 0.02Hz for T300/VE and T700/VE:F

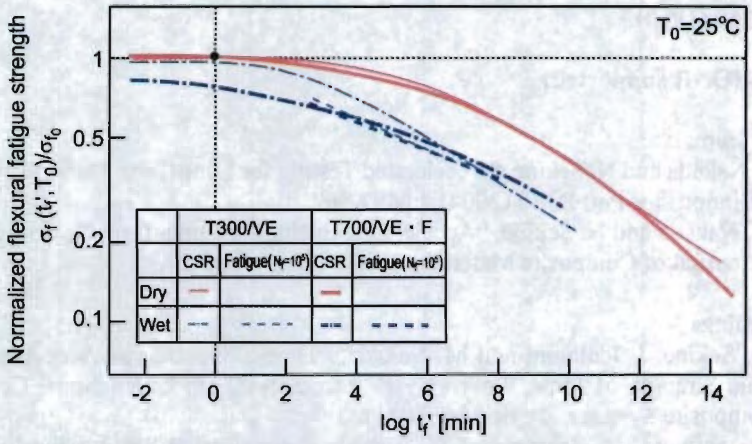

Fig.10 Normalized flexural fatigue strength for T300/VE and T700/VE:F

4. Conclusion

The prediction of long-term fatigue life of innovative CFRP laminates for marine use under temperature and water environments were performed by our developed accelerated testing methodology based on the time-temperature superposition principle (TTSP). The three-point bending CSR and fatigue tests for three kinds of CFRP laminates at three conditions of water absorption were carried out at various temperatures and loading rates. As the results, the flexural fatigue strength of these CFRP laminates strongly depends on water absorption as well as time and temperature, however scarcely depends on the number of cycles to failure. The mater curves of fatigue strength for these CFRP laminates are constructed by using the test data based on TTSP. It is possible to predict the long term fatigue life for these CFRP laminates under an arbitrary temperature and water absorption conditions by using the master curves. Furthermore, the degradation rate of fatigue strength of these CFRP laminates is determined only by increasing of time, temperature and water absorption and is independent upon fiber constitutions which are the type, volume fraction and weaves.

NAVY RELEVANCE

The proposed methodology has effectively combined the effects of time, temperature and water absorption on the strength and life of composite materials. It can be confirmed that the methodology is applicable to the innovative CFRP laminates for marine use.

ACKNOWLEDGEMENTS

The authors thank the Office of Naval Research for supporting this work through an ONR award (N000140110949) with Dr. Yapa Rajapakse as the ONR Program Officer. The authors thank Professor

Richard Christensen at Stanford University as the consultant of this project and Toray Industries, Inc. as the supplier of CFRP laminates.

REFERENCES

1. Aboudi, J. and Cederbaum, G., Composite Structures, 12: 243-256 (1989).
2. Sullivan, J. L., Composite Science and Technology, 39: 207-232 (1990).
3. Gates, T., Experimental Mechanics, 68-73 (1992).
4. Miyano, Y., Kanemitsu, M., Kunio, T. and Kuhn, H., J. Composite Materials, 20: 520-538 (1986).
5. Miyano, Y., McMurray, M. K., Enyama, J., and Nakada, M., J. Composite Materials, 28: 1250-1260 (1994).
6. Miyano, Y., K. McMurray, M., Kitade, N., Nakada, M. and Mohri, M., Advanced Composite Materials, 4: 87-99 (1994).
7. Miyano, Y., Nakada, M., and McMurray, M. K., J. Composite Materials, 29: 1808-1822 (1995).
8. Miyano, Y., Nakada, M., McMurray, M. K. and Muki, R., J. Composite Materials, 31: 619-638 (1997).
9. Shen, C. H and Springer, G. S., J. Composite Materials, 10: 2-20 (1976).
10. Kibler, K. G., AGRD Conference Proceedings, 8-1, (1980).
11. Neumann, S. and Marom, G., Polymer Composites, 6: 9-12 (1985).
12. Selzer, R., and Friedrich, K., Composites Part A, 28A: 595-604 (1997).
13. Dow, N. F., Gruntfest, I. J., Space Sciences Laboratory, Structures and Dynamics Operation, T.I.S.R60SD389 (1960).

PUBLICATIONS (ONR supported)

Papers in refereed journals

1. Y. Miyano, M. Nakada and N. Sekine, "Accelerated Testing for Long-Term Durability of GFRP Laminates for Marine Use", Composites Part B, 35 (2004), pp497-502.
2. Y. Miyano, M. Nakada and N. Sekine, "Accelerated Testing for Long-Term Durability of FRP Laminates for Marine Use", Journal of Composite Materials, Vol.39 (2005), pp5-20.

Conference proceedings

1. Y. Miyano, N. Sekine, J. Ichimura and M. Nakada, "Time-Temperature-Water Absorption Dependence of Flexural Fatigue Strength of Plain Woven CFRP Laminates", 6th International Conference on Durability Analysis of Composite Systems, (Riga, May 2004).
2. Y. Miyano, J. Ichimura, N. Sekine and M. Nakada, "Accelerated Testing for Long-Term Durability of Advanced CFRP Laminates for Marine Use", 11th Japan-United States Conference on Composite Materials, (Yonezawa, Sept. 2004).
3. M. Nakada, J. Ichimura, N. Sekine and Y. Miyano, "Time-Temperature-Water Absorption Dependent Fatigue Strength of Plain Woven CFRP Laminates", 11th Japan-United States Conference on Composite Materials, (Yonezawa, Sept. 2004).
4. M. Nakada, J. Ichimura and Y. Miyano, "Long-Term Durability of Plain-Woven CFRP Laminates under Water Conditions", 2nd JSME/ASME International Conference on Materials and Processing 2005 (Seattle, June 2005).
5. E. Hayakawa, J. Ichimura, M. Nakada, Y. Miyano, "Influence of Water Absorption on the Time-Temperature Dependent Flexural Strength of Plain Woven CFRP", 2nd JSME/ASME International Conference on Materials and Processing 2005 (Seattle, June 2005).
6. Y. Miyano, J. Ichimura and M. Nakada," Accelerated Testing for Long-Term Durability of Advanced CFRP Laminates for Marine Use", 15th International Conference on Composite Materials,(Durban, June 2005)
7. M. Nakada, J. Ichimura, J. Noda and Y. Miyano, "Time-Temperature-Water Absorption Dependent Flexural Strength of CFRP Laminates for Marine Use", 5th International Conference on Mechanics of Time Dependent Materials, (Karuizawa, October 2005).

Part II : Environmental effects on damage tolerance performance of CFRP laminate for marine use

Isao Kimpara and Hiroshi Saito

Materials System Research Laboratory, Kanazawa Institute of Technology, 3-1 Yatsukaho, Hakusan, Ishikawa 924-0838, Japan

ABSTRACT

In multiaxial stitched CFRP laminates, it is thought that the existences of knitting fibers in between layers and gaps between carbon fiber bundles etc., which are configurations different from conventional unidirectional and woven laminates, significantly affect the interlayer fracture properties. Besides, objective large-scale structures are affected by environment such as variable temperature and humid, thus the interlayer fracture properties might become more complicated. In this study, Mode I and Mode II interlaminar fracture toughness and the crack growth property under fatigue, thermal and water environments of multiaxial stitched CFRP laminates for innovative marine composites were investigated.

INTRODUCTION

Damage tolerance is very important in structural use of composites. A better understanding of the effects of damage on the performance of composite structures and better analytical tools and methodologies to predict this performance are required to make composite structures more economical and trustworthy, and to therefore allow composites to be utilized to their maximum potential. Damage growth processes of composite materials are very complicated and modeling of such processes has not been easy. However, the recent advances in experimental and computational mechanics has made it easier to propose a more realistic and accurate damage modeling even for such a complicated damage modes in composite materials, if the both approaches are properly combined and fused.

The damage tolerance performance is comparatively evaluated in terms of compressive strength after impact (CAI) and Mode I and Mode II delamination toughness. The durability is evaluated for some selected material systems through damage process observation under both static and repeated loading and Mode I and Mode II fatigue delamination growth. In addition, the effect of environment such as temperature and water absorption on interlaminar fracture toughness is evaluated. In the past reports, CAI and post impact fatigue (PIF) results of candidate materials were reported. In this report, the environmental effects on Mode I and Mode II interlaminar fracture toughness and PIF property were focused.

MATERIALS

There has been a big technological gap between aerospace and marine composite materials not only in reinforcing fibers and matrix but also in manufacturing process. Marine composite materials have so far been limited mainly to E-glass fiber and unsaturated polyester resin based on cold curing contact molding process. The fiber form has also been limited mainly to thick woven fabric and chopped strand mat. The application of advanced composite materials in the marine industry has been limited to high-performance racing yachts, high-speed power boats and some surface effect ships because of the high material cost and the sophisticated manufacturing process. However there is now more than sufficient evidence to show that properly engineered advanced composite structures will produce much lighter and much more durable large-scale marine vehicles by means of rational choice of structural concept and manufacturing process. We note that several developments have recently been done which might be able to give cost effective and affordable new type of reinforcements and core materials for marine composite structures based on vacuum assisted resin transfer molding (VARTM) process. Figure 1(a) shows the schematic image of VARTM setting. It is generally more difficult to flow the resin in carbon fiber than in glass fiber. From this reason, a meshing sheet was set on the peel cloth to flow the resin faster in carbon fiber tow. The resin was flown in a meshing sheet at first, and then was flown in carbon fiber, as shown in Fig.1(b).

The candidate material is a new type of multi-axial stitched preform as shown in Fig.2, T700S-12K,

developed by Toray Industries, Inc., which consists of 12K yarns of high tensile strength carbon fiber. The candidate fabric is much stronger than the conventional T300-3K fabric because of its intrinsic high tensile strength and smooth warping of fiber yarns due to flatness of the yarn. Furthermore all yarns in this fabric have no-crimp, thus high mechanical properties which fiber originally has can be performed. CFRP laminates are fabricated based on VARTM with multi-axial stitched preforms and vinylester (VE) as matrix resin.

Stacking sequence of CFRP laminate was $[(0°/90°)/(90°/0°)]_{2Symm}$. Here, (0°/90°) means one layer of double-axial stitched fabric. For initial crack, fluorocarbon polymer film with 25μm thickness was inserted in neutral plane of this laminate.

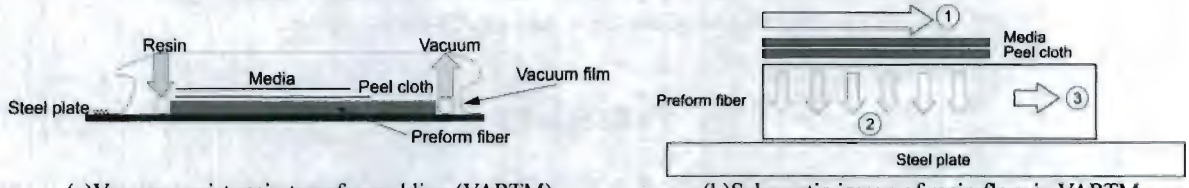

(a)Vacuum assist resin transfer molding (VARTM) (b)Schematic image of resin flow in VARTM

Fig.1 Schematic images of the vacuum assisted resin transfer molding (VARTM) method.

(b)Multi-axial stitched preform

Fig.2 The configurations of candidate material.

APPROACH

Mode I and Mode II interlaminar fracture toughness tests were conducted with the jig based on Japanese Industrial Standard (JIS) K 7086 "Testing methods for interlaminar fracture toughness of carbon fibre reinforced plastics". All tests were conducted by servohydraulic testing machine (Shimadzu EHF-FB5KN-10LA, load capacity 5 kN).

(1) Mode I and Mode II fatigue interlaminar fracture toughness tests

Dimension of the specimens of double cantilever bending (DCB) test for Mode I and end notched flexure (ENF) test for Mode II are shown in Fig.3 and Fig.4 respectively. In ENF test, Nichrome wire with 0.2mm thickness was inserted between crack surfaces in order to decrease contact resistance in between crack surfaces.

Crack growth rate based on Paris's law is evaluated in DCB and ENF fatigue tests. In this study, decreasing fatigue tests under constant COD and CSD were conducted. Decreasing rate of energy release rate is defined as equation (1).

$$\frac{1}{G}\cdot\frac{dG}{da}=2C \tag{1}$$

Here, $2C$ is the ratio of energy release rate change to crack growth length.

For Mode II test, the following two expressions are obtained.

$$\frac{dG_{\mathrm{II}\max}}{da}=\frac{3}{8BH}\left(2P_{\max}\lambda\frac{dP_{\max}}{da}+P_{\max}^{2}\frac{d\lambda}{da}\right) \tag{2}$$

$$\frac{d\lambda}{da}=\frac{3a}{E_L BH^2} \tag{3}$$

Equation (2) is substituted for (3) and divided by G_{IImax}, and that is substituted for (1), then equation (4) is obtained.

$$\frac{1}{P_{\max}}\frac{dP_{\max}}{da} = c - \frac{1}{a} \tag{4}$$

In the case of constant displacement test, dP_{max}/da equals 0 and decreasing rate, C, is obtained by $1/a$.
For Mode I test, following equation is defined by Hojo et al.[1)]

$$C = -\frac{n+1}{2a} \tag{5}$$

Here, n is slope value of the chart of the relation between crack length and COD compliance.

The range of energy release rate in fatigue test is calculated with stress ratio, R, as following equation.

$$\Delta G = G_{\max}(1 - R^2) \tag{6}$$

Crack growth rate, da/dN, is calculated by ΔG and crack growth length, δ for DCB test and for ENF test respectively. Relation between ΔG and da/dN is drawn as double logarithmic chart. From linear range except upper and bottom energy release rate range in this chart, approximation equation as well as equation (6) is obtained.

$$\frac{da}{dN} = C\Delta G^m \tag{7}$$

Here, C and m are material properties. Especially m is a parameter of crack growth rate.

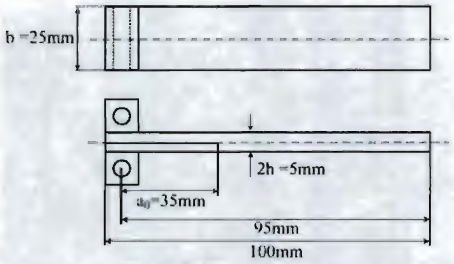

Fig.3 DCB specimen.

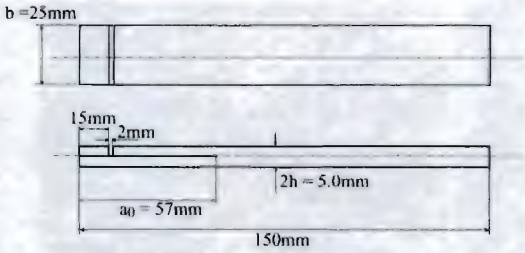

Fig.4 ENF specimen.

(2) Interlaminar fracture toughness test under thermal condition

First, dynamic visco-elastic properties of vinylester resin which is the matrix resin in this study was evaluated, and glass transition point (T_g) 118.5°C was obtained. Thermal condition was decided as 60°C, 80°C and 100°C based on this T_g. Fatigue test was conducted under condition of 80°C only. All tests under thermal condition were conducted with thermostatic chamber, and temperature in chamber was measured by thermocouple.

(3) Interlaminar fracture toughness test under water condition

Saturation water absorption ratio of target CFRP laminate was 0.45wt% under 95°C for approximately 300 hours. Therefore all tests under water condition were conducted after 2 weeks (336 hours) soak in water bath under 95°C condition. Specimens after soaking are named as "Wet" specimens. On the other hand, specimens dried under 150°C for 2 hours after soaking until water absorption ratio becomes 0.1wt% were also prepared. These specimens are named as "Wet+Dry" specimens. Wet specimens soaked were held in water bath under room temperature, and tested in plastic water bag under room temperature.

RESULTS AND DISCUSSIONS

1. The effects of temperature on interlaminar fracture toughness

1.1. Mode I static test under thermal condition

R-curve chart is shown in Fig.5. It was found that both energy release rate (G_{IR}) and variation of G_{IR} increased with increasing of temperature. Figure 6 shows average values of G_{IC} and G_{IR}. From this figure, it is clear that G_{IC} hardly varied though G_{IR} tended to increase with increasing of temperature. As the reason why G_{IC} was hardly varied at any temperatures, the effect of existing of knitting fibers is considered. By the observation of crack tip region, it is found that knitting fibers played a role as bridge with upper and lower cantilevers in the initial stage of crack growth.

On the other hand, variation of G_{IR} at higher temperature is discussed by the fiber bridging in the crack growth stage. The amount of fiber bridging at 100°C was much than that at room temperature. In addition, however interface fracture between fiber and matrix was observed at room temperature as shown in Fig.7 (a), resin fracture was mainly observed at 100°C as shown in Fig.7 (b). Consequently, it is thought that much fiber bridging and matrix fractures caused higher G_{IR} at higher temperature.

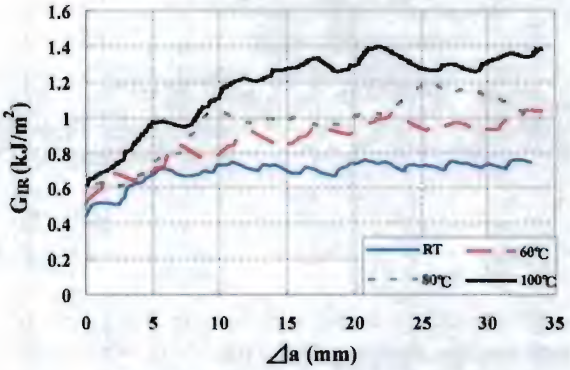

Fig.5 R-curve of Mode I DCB test.

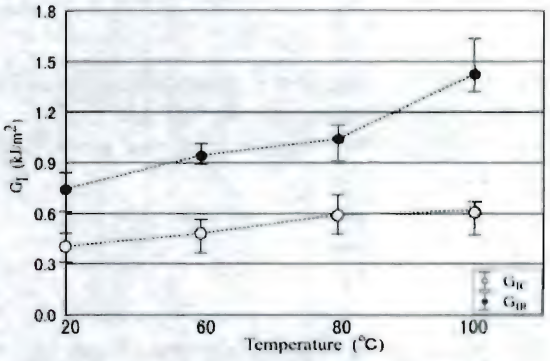

Fig.6 Average values of G_I at variable temperatures.

(a) Room temperature (x1000)

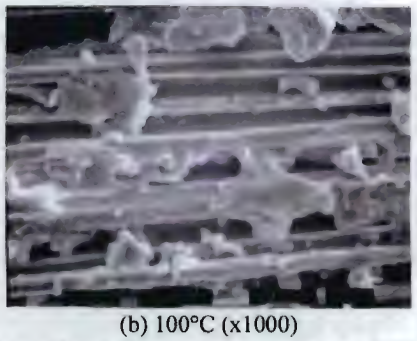

(b) 100°C (x1000)

Fig.7 Scanning electron microscopic photographs of fracture surface of Mode I tests at room temp. and 100°C.

1.2. Mode II static test under thermal condition

R-curve chart is shown in Fig.8. Energy release rate (G_{II}) decreased with increasing of temperature. Additionally G_{II} at higher temperature showed larger variation. Figure 9 shows average values of G_{IIC} and G_{IIR}. From this figure, it is clear that G_{IIC} showed significant decrease with increasing of temperature. G_{IIC} at 100°C showed about 53% decrease compared with that at room temperature. Conversely, the influence of the temperature was a little except at 100°C at which G_{II} showed slightly decrease.

These results were discussed by the observation of fracture surfaces as shown in Fig.10. Much hackle fractures were observed in the specimen at room temperature, thus it was found that brittle resin fracture occurred. In contrast, no hackle fracture was observed in the specimen at 100°C. Normally, hackle fracture causes the phenomenon so called interlocking in which hackle engages each other and contact resistance between fracture surfaces increases, and this phenomenon makes G_{II} increase[2]. Therefore it is thought that G_{IIC} at 100°C decreased by decreasing of hackle fracture. However in this study, G_{IIR} was hardly affected by the temperature variation.

Figure 11 shows knitting fibers which were broken by interlaminar delamination growth. Because the dimension of broken knitting fibers are much larger than that of hackle fracture, for example thickness of knitting fibers are about 200μm and that of hackle is about 10μm, it is thought that the effect of knitting fibers on the contact resistance between fracture surfaces is much larger than that of hackle fracture. Therefore it is

thought that G_{IIR} in crack growth stage is not affected by the contact resistance of hackle fracture but rather by that of knitting fibers. Conversely broken knitting fibers tend to accelerate the crack growth, thus large variation was observed in R-curve chart.

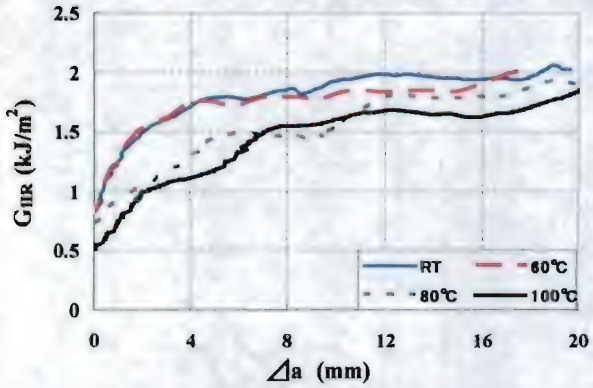

Fig.8 R-curve of Mode II ENF test.

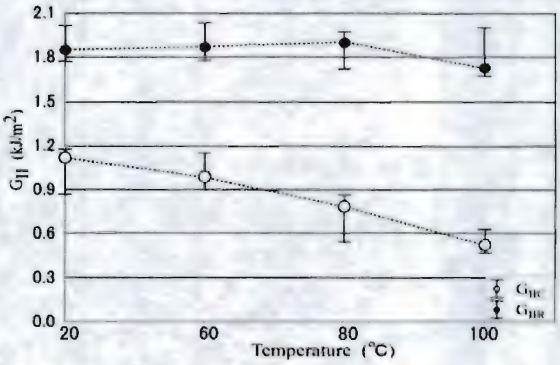

Fig.9 Average values of G_{II} under variable temperatures.

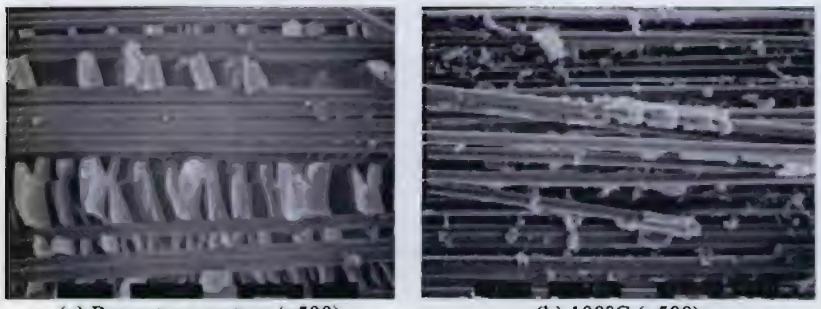

(a) Room temperature (x500) (b) 100°C (x500)

Fig.10 Scanning electron microscopic photographs of fracture surface of Mode II tests at room temp. and 100°C.

Fig.11 Scanning electron microscopic photograph of breakage of knitting fiber. (x60)

1.3. Mode I fatigue test under thermal condition

In Mode I fatigue test under thermal conditions, fatigue load gradually decreased with increasing of cycles at both room temperature and 80°C. Decreasing rate of fatigue tests, $2C$, was from -0.05mm^{-1} to -0.12mm^{-1} at room temperature, and from -0.05mm^{-1} to -0.10mm^{-1} at 80°C. These values are within the range of decreasing rate defined by ASTM E647-88, $2C$ > -0.16mm^{-1}, and it can be said that decreasing fatigue tests were approved.

Relation between crack growth rate and increment of crack length is shown in Fig.12. However local variation of crack growth rate was observed in this figure, it is thought that this is caused by the existence of knitting fiber, such as shown in static Mode I test. Figure 13 shows a chart of the relation between range of energy release rate and crack growth rate. Solid lines in this figure are the approximation line in linear range of this chart. From the slope of approximation lines, it was found that crack growth rate at room temperature was higher than that at 80°C. As well as static test, interface fracture was observed at room temperature as shown in Fig.14 (a), however, resin fracture was mainly observed at 80°C as shown in Fig.14 (b). Therefore it is thought that this change of fracture morphology caused delay of crack growth rate at 80°C.

1.4. Mode II fatigue test under thermal condition

In Mode II fatigue test under thermal conditions, fatigue load gradually decreased with increasing of cycles at room temperature. On the contrary, after rapid load decreasing, load decreased linearly at 80°C. Therefore it is thought that decreasing fatigue tests were not approved at 80°C. At room temperature, decreasing rate of fatigue tests, $2C$, was from -0.50mm^{-1} to 0.25mm^{-1}, which is within the range of decreasing rate defined by ASTM E647-88, $2C$ > -0.16mm^{-1}. Therefore it can be said that decreasing fatigue test was approved only at room temperature condition.

Relation between crack growth rate and increment of crack length is shown in Fig.15. In the test at 80°C, linear relation between crack growth rate and increment of crack length was not observed. It is thought that this phenomenon was caused by sudden breakage of knitting fibers such as shown in static Mode II test. Relation between crack growth rate and increment of crack length is shown in Fig.16. However linear relation was approved at room temperature, it was not approved at 80°C. On the other hand, threshold energy release rate

range at room temperature was about 420J/m^2 and that at 80°C was about 175J/m^2, thus energy release rate range at which crack growth starts at 80°C is lower than that at room temperature. Figure 17 shows photographs of fracture surface. Hackle fractures were observed at both room temperature and 80°C, however, the size of hackle at room temperature was smaller than that of 80°C. It is thought that this difference of fracture morphology caused different crack growth rate between at room temperature and 80°C.

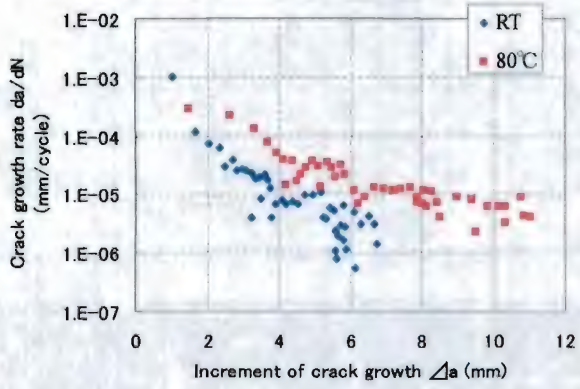

Fig.12 Relation between crack growth rate and increment of crack length of Mode I DCB fatigue test at room temp. and 80°C.

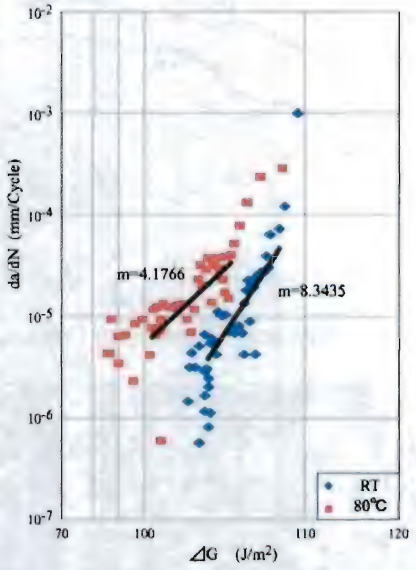

Fig.13 Relation between *da/dN* and Δ*G* of Mode I DCB fatigue test at room temp. and 80°C.

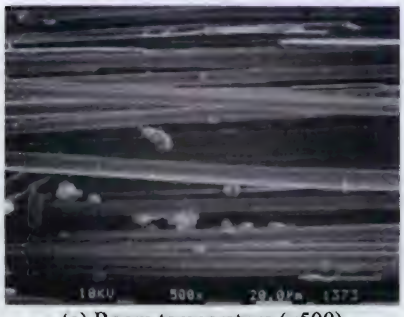

(a) Room temperature (x500)

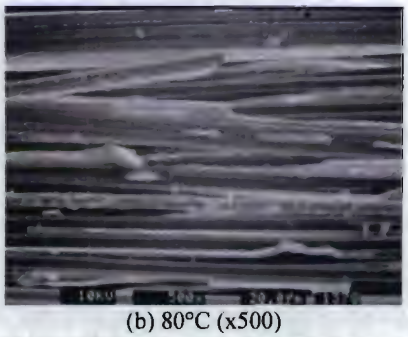

(b) 80°C (x500)

Fig.14 Scanning electron microscopic photographs of fracture surface of Mode I fatigue tests under room temp. and 80°C.

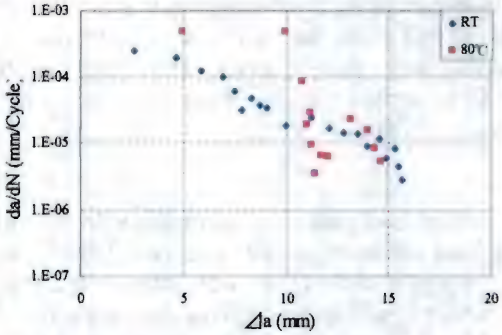

Fig.15 Relation between crack growth rate and increment of crack length of Mode II ENF fatigue test at room temp. and 80°C.

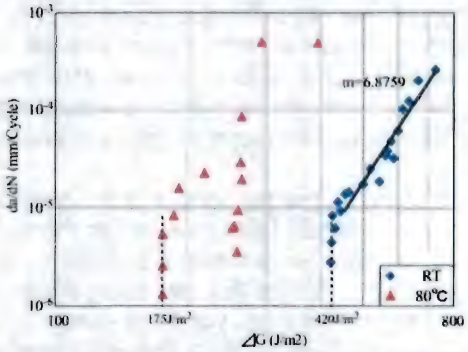

Fig.16 Relation between *da/dN* and Δ*G* of Mode II ENF fatigue test at room temp. and 80°C.

(a) Room temperature (x500)

(b) 80°C (x500)

Fig.17 Scanning electron microscopic photographs of fracture surface of Mode II fatigue tests at room temp. and 80°C.

2. The effects of water absorption on interlaminar fracture toughness

2.1. Mode I static test under water condition

R-curve chart is shown in Fig.18. From this chart, it is found that the effect of water absorption on G_I was small. Figure 19 shows average values of G_{IC} and G_{IR} under Dry, Wet and Wet+Dry conditions. G_{IC} under Wet condition slightly decreased from that under Dry condition, and slightly recovered in Wet+Dry condition. Conversely G_{IR} under Wet condition slightly increased from that under Dry condition, and decreased again in Wet+Dry condition. Consequently, it can be said that the effect of water absorption on G_I is small.

These results are discussed by the observation of edge surface. More fiber bridging was observed in Wet and Wet+Dry conditions than in Dry condition. In fracture surfaces of specimens under all conditions observed by scanning electron microscope as shown in Fig.20, interfacial fracture was observed in all specimens. Generally it is well known that interface between fiber and matrix is damaged by water absorption[3-6]. It is thought that interface between fiber and matrix was weakened by water absorption, however, main fracture morphology was not changed thus G_I was not affected by water absorption.

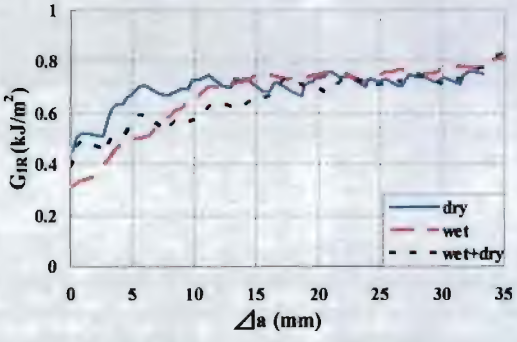

Fig.18 R-curve of Mode I DCB test.

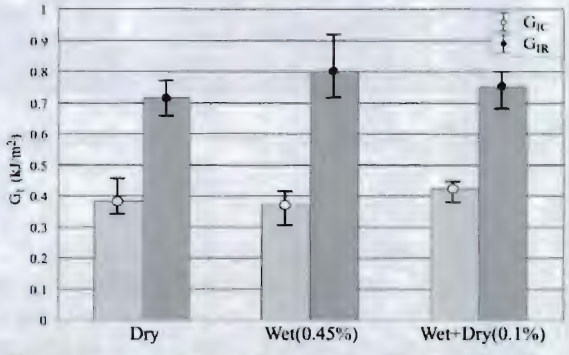

Fig.19 Average values of G_I under Dry, Wet and Wet+Dry conditions.

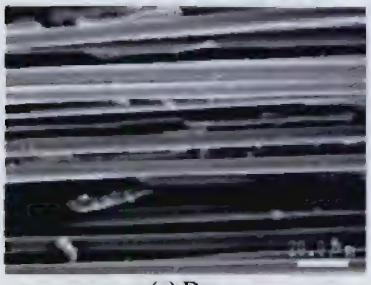

(a) Dry

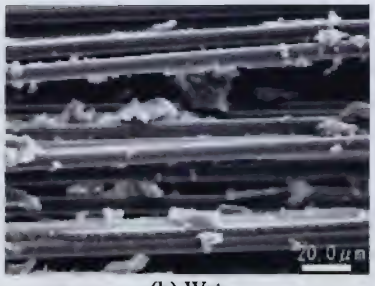

(b) Wet

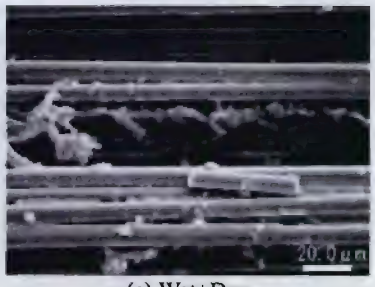

(c) Wet+Dry

Fig.20 Scanning electron microscopic photographs of fracture surface of Mode I tests under Dry, Wet and Wet+Dry conditions.

2.2. Mode II static test under water condition

R-curve chart and average values of G_{IIC} and G_{IIR} are shown in Fig.21 and Fig.22 respectively. G_{IIC} and

G_{IIR} under Wet condition decreased from that of Dry condition, and slightly increased in Wet+Dry condition. These results are discussed by the observation of fracture surface as shown in Fig.23. All specimens showed interfacial fracture as well as Mode I tests, and hackle fracture was also observed. Especially Dry and Wet+Dry specimens showed remarkable hackle fracture, so that it was found that resin condition in these two cases was brittle. Therefore it is thought that brittleness was disappeared in water condition, however, it was recorvered in Wet+Dry condition.

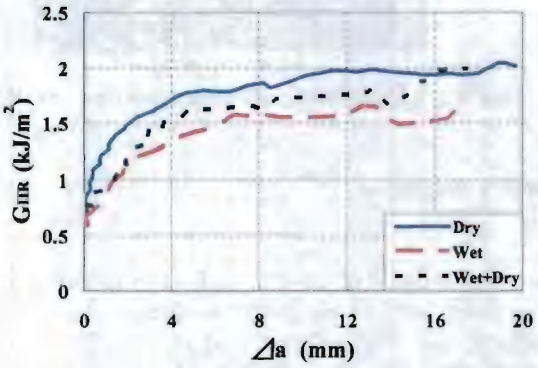

Fig.21 R-curve of Mode II ENF test.

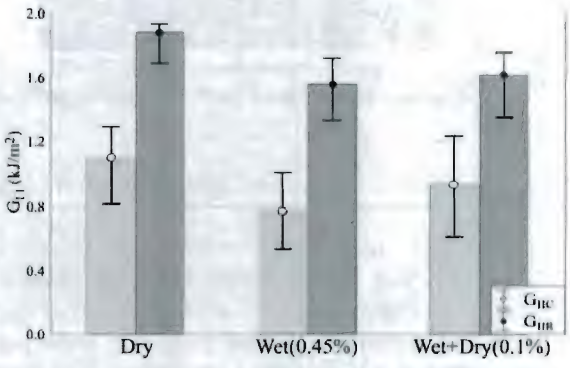

Fig.22 Average values of G_{II} under Dry, Wet and Wet+Dry conditions.

(a) Dry (b) Wet (c) Wet+Dry

Fig.23 Scanning electron microscopic photographs of fracture surface of Mode II tests under Dry, Wet and Wet+Dry conditions.

2.3. Mode I fatigue test under water condition

In Mode I fatigue test under water condition, fatigue load gradually decreased with increasing of cycles in all conditions. In these cases, decreasing rate of fatigue tests, $2C$, was from -0.06mm^{-1} to -0.12mm^{-1} under Wet condition and from -0.05mm^{-1} to -0.12mm^{-1} under Wet+Dry condition. These values are within the range of decreasing rate defined by ASTM E647-88, $2C$ > -0.16mm^{-1}, and it can be said that decreasing fatigue tests were approved for all test conditions.

Relation between crack growth rate and increment of crack length is shown in Fig.24. All tests showed almost same curves. Figure 25 shows a chart of the relation between range of energy release rate and crack growth rate. Solid lines in this figure are the approximation line in linear range of this chart. From the slope of approximation lines, it was found that crack growth rate under Wet condition slightly increased from that under Dry condition, and slightly decreased under Wet+Dry condition. As well as static test, interface fracture was observed in all conditions as shown in Fig.26. From these results, the effect of water absorption was small in Mode I fatigue test.

2.4. Mode II fatigue test under water condition

In Mode II fatigue tests under water condition, decreasing rate of fatigue tests, $2C$, was from -0.017mm^{-1} to -0.06mm^{-1} under Wet condition and from -0.018mm^{-1} to -0.045mm^{-1} under Wet+Dry condition. These values are not within the range of decreasing rate defined by ASTM E647-88, $2C$ > -0.16mm^{-1}, and it can be said that decreasing fatigue test was not approved.

Relation between crack growth rate and increment of crack length is shown in Fig.27. In Wet and Wet+Dry tests, crack growth rate showed large variation. Relation between crack growth rate and increment of crack length is shown in Fig.28. However linear relation was not approved in Wet and Wet+Dry tests, threshold

energy release rate range in Wet condition slightly recovered by drying.
Figure 29 shows photographs of fracture surface of specimens under each condition. Interfacial fracture and hackle fracture were observed in all conditions. Wet+Dry specimen showed clearer hackle fracture than Wet one, so that it was found that resin condition in Wet+Dry specimen was brittle. Therefore it is thought that brittleness of resin under Wet condition was recorvered by drying.

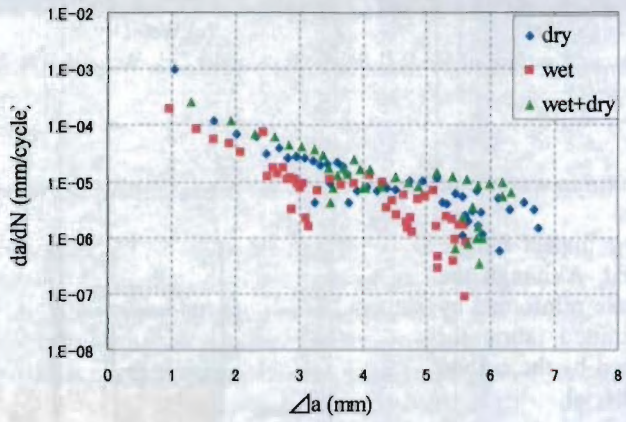

Fig.24 Relation between crack growth rate and increment of crack length of Mode I DCB fatigue test under Dry, Wet and Wet+Dry.

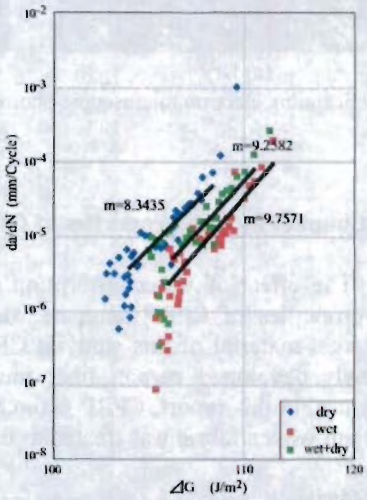

Fig.25 Relation between *da/dN* and Δ*G* of Mode I DCB fatigue test under Dry, Wet and Wet+Dry.

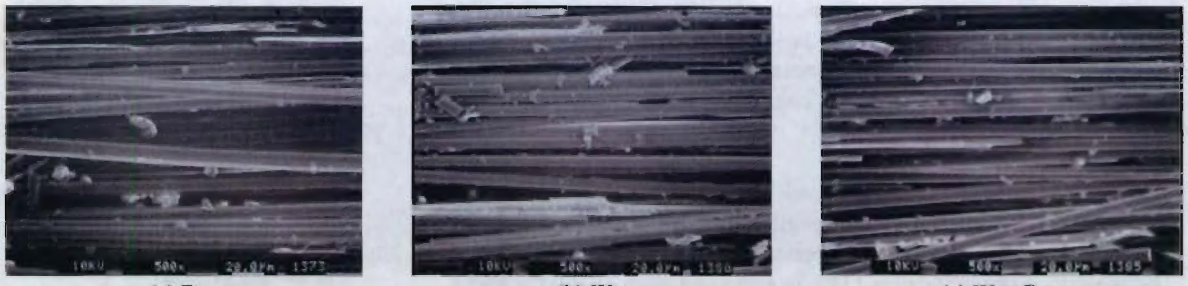

(a) Dry (b) Wet (c) Wet+Dry

Fig.26 Scanning electron microscopic photographs of fracture surface of Mode I fatigue tests under Dry, Wet and Wet+Dry.

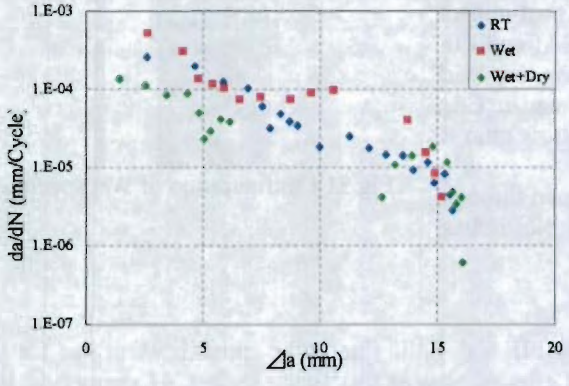

Fig.27 Relation between crack growth rate and increment of crack length of Mode II ENF fatigue test under Dry, Wet and Wet+Dry.

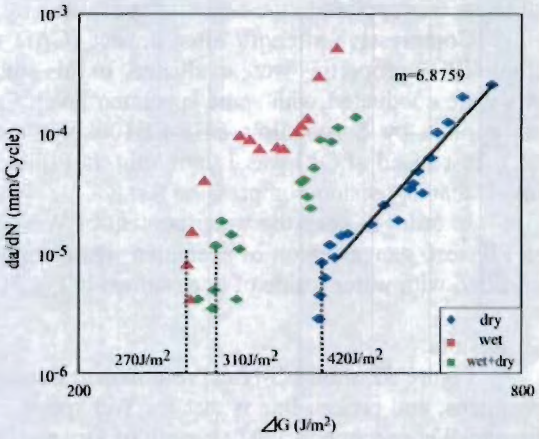

Fig.28 Relation between *da/dN* and Δ*G* of Mode II ENF fatigue test under Dry, Wet and Wet+Dry.

(a) Dry (b) Wet (c) Wet+Dry

Fig.29 Scanning electron microscopic photographs of fracture surface of Mode II fatigue tests under Dry, Wet and Wet+Dry.

3. Post impact fatigue properties of CFRP laminate in water condition

The effect of water absorption on the post impact fatigue (PIF) properties of CFRP laminate was evaluated. Although the main target material of this study is CFRP laminate reinforced by the newly developed carbon fiber multi-axial knitted fabric for marine use, in this report, CFRP laminate reinforced by the carbon fiber plain woven fabric was treated as the base material.

3.1. Materials

Material evaluated was T300B plain woven / vinylester CFRP laminate, which is molded by VARTM process. The number of ply is 9. CFRP laminate was cured at room temperature for 24 hours in molding process, and post-cured at 150°C for 2 hours. Specimens were soaked in water at 95°C for 120 hours in order to make reach the saturation water content of 0.6wt%. Specimens after soaking were named as "Wet", as contrasted with "Dry" ones.

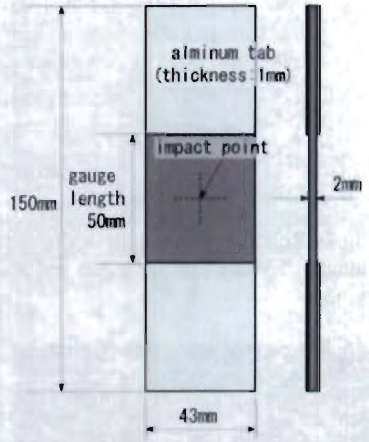

Fig.30 Specimen geometry for CAI and PIF tests.

3.2. Approach

Schematic of specimen used is shown in Fig.30. Length of specimen is 150mm and gauge length is 50mm. Width is 43mm. A drop weight with a steel semi-spherical tip was used as an impactor. The weight of impactor was 1113.5g and the radius of the tip was 8 mm. The specimen was mounted between the supporting steel plates with cut-out hole of 15mm in radius, and is given impact energy directly using the impactor. Impact loading of 1J per unit thickness was applied to the center of specimens by impactor.

Compressive strength after impact (CAI) and post-impact fatigue (PIF) properties were evaluated. In this study, CAI and PIF tests were conducted with same specimen level. Compressive load was applied by Servopulser EHF-EB100kN-20L (Shimadzu Co., Ltd.). Test speed of CAI was 1.0mm/min. In PIF tests, stress ratio R was -1, that is, tension-compression test.

In order to keep the water content of Wet specimen through the PIF test, gauge region of specimen was covered by plastic bag and filled with water inside of it, as shown in Fig.31.

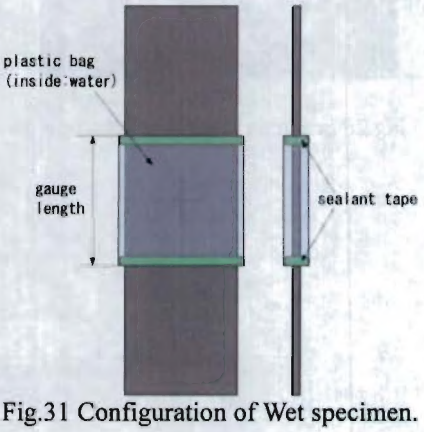

Fig.31 Configuration of Wet specimen.

3.3. Results

Figure 32 shows S-N curve obtained through the PIF test. Solid line is the approximation line for Dry specimens, and broken line is that for Wet specimens. Leftmost plots in this figure show CAI strength of both Dry and Wet specimens. CAI strength of Dry and Wet specimen showed almost same value. In the fatigue test, Dry showed longer fatigue life than Wet, however, the difference between these two was small. Therefore for T300B plain woven CFRP laminate, the effect of water absorption on PIF properties was small.

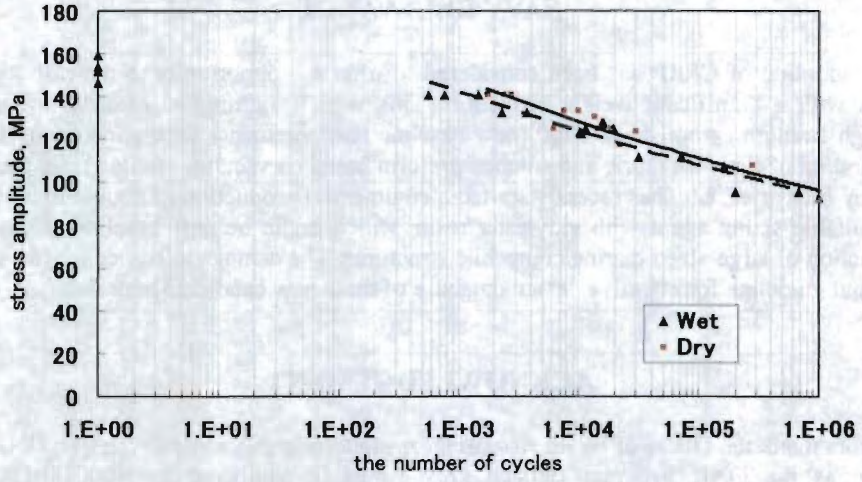

Fig.32 Fatigue strength under water absorption condition for T300B plain woven CFRP laminate.

CONCLUSIONS

In this study, Mode I and Mode II interlaminar fracture toughness and the crack growth property under fatigue, thermal and water environments of multiaxial stitched CFRP laminates for innovative marine composites were investigated. Main accomplishments of this study are following.

(1) The effects of temperature

G_{IC} hardly varied though G_{IR} tended to increase with increasing of temperature. In Mode II fracture toughness tests, G_{IIR} was not affected by temperature, however, G_{IIC} showed significant decrease with increasing of temperature. Crack growth rate under fatigue condition of Mode I fracture toughness tests decreased with increasing of temperature. In Mode II tests, the crack growth rate da/dN versus the variation of energy release rate ΔG curve showed large variation and Paris's law was not held. However, it was obvious that threshold energy release rate range ΔG_{th} was significantly decreased with increasing of temperature. From the observations of end face and fracture surface, interface fracture between fiber and matrix was observed under room temperature whereas resin fracture was dominant under higher temperature condition.

(2) The effects of water absorption

In order to evaluate the effect of water environment, CFRP laminates were soaked in a hot water bath in 95°C for 300 hours till amount of water absorption became 0.45w% which is the saturated water content. G_{IC} was barely decreased with water absorption though G_{IR} tended to increase, and both G_{IC} and G_{IR} were almost recovered by drying after water absorption. In Mode II tests, both G_{IIC} and G_{IIR} decreased by water absorption and slightly but incompletely recovered by drying after water absorption. Crack growth rate under cyclic loading of Mode I tests became faster with water absorption, and slightly recovered by drying after water absorption. In Mode II tests, however da/dN versus ΔG curve showed large variation and Paris's law was not held, ΔG_{th} was recovered by drying after water absorption. From the observations of end face and fracture surface, it was found that interface was damaged and perfectly fractured by water absorption.

(3) The effects of existence of knitting fibers

In Mode I tests, because knitting fibers played a role of fiber-bridge when crack growth started, G_{IC} tended to hardly be affected by temperature and water environments. Conversely in Mode II, the effect of knitting fibers broken after crack propagation on contact resistance between fracture surfaces was larger than that of hackle fractures. Thus the environmental effects on interlaminar fracture toughness in Mode II were hardly cleared and Paris's law was not held.

(4) Post impact fatigue properties of CFRP laminate in water condition

The effect of water absorption on the post impact fatigue (PIF) properties of T300B plain woven CFRP laminate was evaluated. CAI strength and PIF property of this material were not affected by water absorption condition.

NAVY RELEVANCE

Massive adoption of CFRP has been considered to offer the opportunity to develop high performance naval structures with a significant weight reduction. This work is aiming at affordable and cost-effective utilization of high strength carbon fiber T700 (new baseline reinforcement) for marine composite structures in the new configuration of flat yarn fabric and stitched preform based on vacuum assisted resin transfer molding.

The Toray Industries, Ltd. has recently started a commercial production of double-axial stitched preform of T700 with suitable sizing agent with vinylester resin, which might be new baseline reinforcement for the possible construction of large-sized marine composite structures. The damage tolerance evaluation methodology will give a rational guideline for effective design database of these new candidate materials.

ACKNOWLEDGEMENT

The authors thank the Office of Naval Research for supporting this work through an ONR award with Dr. Yapa Rajapakse as the ONR Program Officer. Our award is numbered to N000140110949 and titled "Long-Term Durability and Damage Tolerance of Innovative Marine Composites (NICOP)". The authors thank Professor Richard Christensen, Stanford University as the consultant of this project.

REFERENCES

1. M. Hojo, K. Tanaka, K. Kenmochi, Materials System, 8, pp.89-100 (1989)
2. K.S. Kim, W.X. Wang, Y. Takao, Proc. the JSASS/JSME Structures Conf., 40, pp.77-80 (1998)
3. I.T. Chou, I. Kimpara, K. Kageyama, I. Ohsawa, J. Japan Society for Composite Materials, 19, 2, pp.46-54 (1993)
4. Y. Nakai, T. Kadowaki, C. Hiwa, J. Japan Society of Mechanical Engineers Part A, 66, 649, pp.47-54 (2000)
5. S. Matsuda, M. Hojo, S. Ochiai, J. Japan Society of Mechanical Engineers Part A, 64, 622, pp.205-211 (1998)
6. Y. Nakai, T. Kadowaki, C. Hiwa, J. Japan Society of Mechanical Engineers Part A, 64, 619, pp.40-45 (1998)

List of Publications after January 2004 (Supported by ONR)

1. I. Kimpara and H. Saito, Evaluation of Impact Damage Mechanism of Multi-axial Stitched CFRP Laminate, Composites Part A, under referee (September 2004).
2. I. Kimpara, H. Saito and K. Yamaguchi, Impact Damage and Post-Impact Fatigue Behavior of CFRP Laminates for Marine Use, Proc. The 9th European-Japanese Symposium on Composite Materials (Hamburg, May 2004).
3. H. Saito and I. Kimpara, Impact Damage and Its Growth Behavior of Multi-axial Stitched CFRP Laminates, Proc. The 6th China-Japan-US Joint Conference on Composite Materials, pp.31-35 (Chongqing, June 2004).
4. H.Saito, I.Kimpara, Impact damage and its growth behavior of multi-axial stitched CFRP laminates, The Sixth China-Japan-US Joint Conference on Composites Proceedings, pp.31-36, (Yonezawa, Sept. 2004).
5. H.Saito, I,Kimpara, Observation and evaluation of impact damage on plain woven CFRP laminate, Fifth Joint Canada-Japan Workshop on Composites, pp.451-458, (Yonezawa, Sept. 2004).
6. H.Saito, I,Kimpara, Damage Progression of Impact Damaged Multi-Axial Knitted CFRP Laminate for Marine Use, to be published on 15th International Conference on Composite Materials,(Durban, June 2005)